Int. J. Electrochem. Sci., 15 **(2020)** 7272 – 7281, doi: 10.20964/2020.08.23

International Journal of
ELECTROCHEMICAL
SCIENCE
www.electrochemsci.org

In Situ Surface Decoration of Single-Wall Carbon Nanohorn with Pt/MnO_2 and its application for Supercapacitors

Jie Huang, Yuting Wang, Hangchun Deng, Jianfa Chen, Jianhua Ding and Chunyan Wang**

School of Chemistry, Biology and Material Science, East China University of Technology, Nanchang 330013, P.R. China
*E-mail: chywang9902@163.com, jhding@ecut.edu.cn

Received: 2 April 2020 / *Accepted:* 23 May 2020 / *Published:* 10 July 2020

Herein, homogeneously dispersed Pt and MnO_2 nanoparticles were anchored to single-walled carbon nanohorns (SWCNHs) to obtain an efficient electrode material for supercapacitors. XPS and TEM analysis of the Pt/MnO_2@SWCNH surface morphology confirms that the SWCNHs exhibit a dahlia-like cluster structure with Pt/MnO_2 nanoparticles embedded in the interstices of the SWCNH horn structure to form a three-dimensional conductive network. This structure not only improves the overall conductivity of the composite but also provides more electron transfer pathways for the MnO_2 nanoparticles. Accordingly, the as-prepared Pt/MnO_2@SWCNH composite displays a high specific capacitance (314.5 F/g at 1 A/g), good cycling stability (86.89% capacitance retention after 1000 cycles at 1 A/g), and remarkable rate performance (254.8 F/g at 10 A/g). Among reported composites of metal oxides, precious metals, and carbon materials, the prepared Pt/MnO_2@SWCNH composite has outstanding electrical properties and is a highly promising candidate as supercapacitor.

Keywords: supercapacitor; single-walled carbon nanohorns; manganese dioxide; platinum

1. INTRODUCTION

Electrochemical techniques are sensitive, stable, and accurate [1–3] and have been widely used in electrochemical biosensors [4–6], fuel cells [7-9], supercapacitors [10], and various other applications. Supercapacitors provide a promising alternative approach to meet the ever-increasing requirements for clean energy storage systems due to their fast energy transportation, high storage capacity, and good recyclability [11, 12]. According to their charge storage mechanism, supercapacitors can be divided into two categories: electrical double-layer supercapacitors (EDLCs) and pseudo-capacitors. The main energy storage mechanism in EDLCs is the charge separation at the interface between electrode and electrolyte, [13] which results in a high charge/discharge rate and a

long recycling life. [14] Correspondingly, EDLCs have the disadvantage of a low energy density, which seriously limits the application in the field of energy storage devices. [15] For pseudo-capacitors, charge storage occurs mainly through a reversible Faradaic redox reaction of the active substance on the electrode surface. Therefore, the specific capacitance of pseudo-capacitors is generally much higher than that of EDLCs. However, irreversible chemical reactions and physical structure damage usually take place in the charge/discharge process of pseudo-capacitors used as active materials, often leading to a poor cycling stability [16]. Hence, improving the specific capacitance and maintaining a long-term cycling stability remain a challenge in the development of supercapacitors.

MnO_2 is attracting more and more attention because of its natural abundance, low cost, environmental benignity, and low toxicity. MnO_2 is also a promising electrode material due its good pseudo-capacitance in neutral electrolytes [17, 18]. The charge storage mechanism of MnO_2 is dominated by the highly reversible Mn^{3+}/Mn^{4+} redox process on the MnO_2 surface. However, the electrical conductivity of MnO_2 is low, leading to a poor rate performance of the electrode, which limits further applications in the supercapacitor field. [19]

Nowadays, carbon materials are used extensively in energy storage devices and high-performance nanocomposites. [20, 21] Single-walled carbon nanohorns (SWCNHs) are new carbon nanotube-related materials with a structure similar to that of roughly spherical nanohorn aggregates. Because of their special geometry, SWCNHs have unique mechanical, chemical, and electrical properties. [22, 23] Furthermore, SWCNHs have a flower-like cluster structure, which provides abundant adsorption and active sites on the surface. This structure is also suitable as the substrate for growing electroactive substances between its horn interstices, which may improve the contact area between active substance and SWCNH substrate, and increase the number of electron transport pathways. Although SWCNHs offer many advantages, to the best of our knowledge, only few studies are reported on applications in supercapacitors. [24]

Herein, the pseudo-capacitor MnO_2 is chosen as the electroactive material, and its conductivity and cycle performance are enhanced using SWCNHs as the conductive substrate. Furthermore, Pt was used to further improve the conductivity of MnO_2. The results proved that both the MnO_2 and Pt nanoparticles were successfully grown on the SWCNH substrate to form a three-dimensional conducting network. The obtained hybrid materials exhibited an excellent electrochemical performance for supercapacitors.

2. EXPERIMENTAL SECTION

2.1 Chemicals

SWCNH was bought from Nanjing XFNano Co., Ltd. The other chemicals were of analytical grade, purchased from Aladdin, and used as received without further purification.

2.2 Preparation of Pt/MnO_2@SWCNH composite

In a typical synthesis, 20 mg of purified SWCNHs were transferred into a round-bottom flask

and dispersed in 40 mL of ethylene glycol by sonication. Subsequently, 100 mg $KMnO_4$ was added to the suspension, which was sonicated for another 20 min. The mixture was refluxed in an oil bath at 135 °C for 3 h. Then, 40 mg of K_2PtCl_6 was added to the mixture under the same reaction conditions. The reaction mixture was centrifuged and washed with distilled water and absolute ethanol for three times. Finally, the obtained product was dried in a vacuum drying oven overnight at 80 °C. Afterwards, the Pt/MnO_2@SWCNH composite was prepared by annealing the product at 500 °C under inert gas atmosphere for 2 h. For comparison, the Pt-free composite MnO_2@SWCNH was prepared by the same procedure without the addition of K_2PtCl_6. The schematic diagram of the composite material preparation is shown in Figure 1.

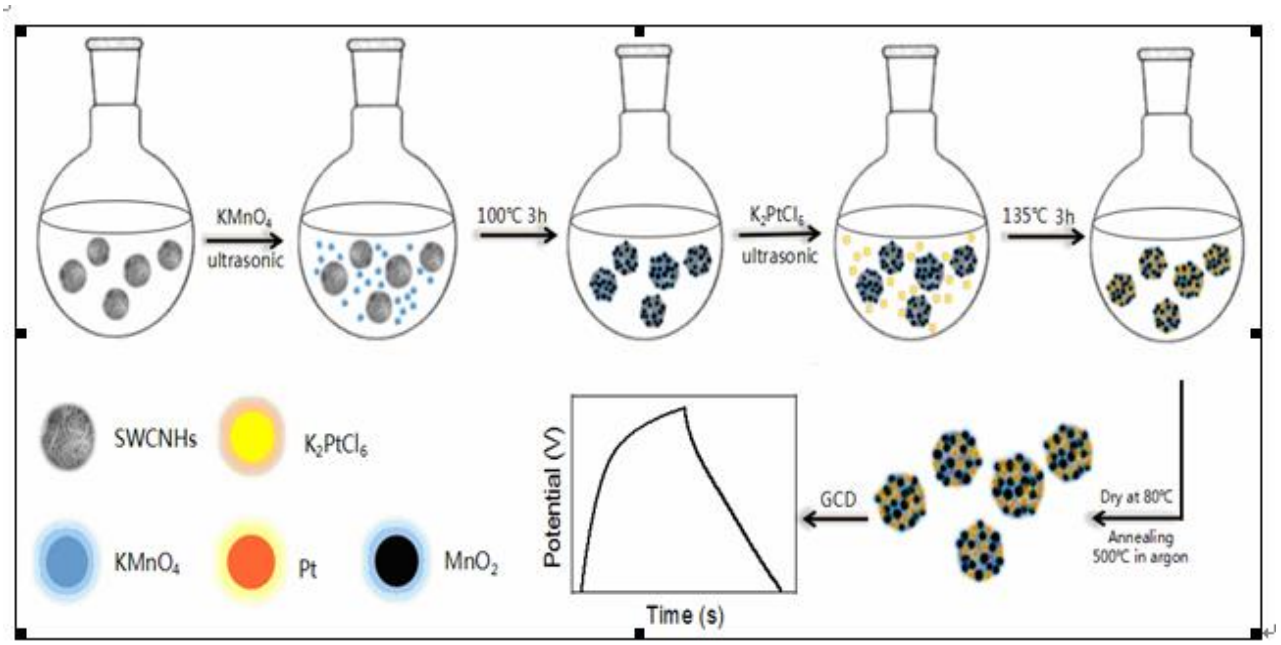

Figure 1. Scheme of the preparation of Pt/MnO_2@SWCNH composites.

2.3 Electrochemical measurements

All the electrochemical measurements were performed on a CHI 660E electrochemical workstation with a three-electrode system in 1.0 mol/L Na_2SO_4 aqueous solution. The working electrode was fabricated by mixing the as-prepared composite powder (80 wt%) with polytetrafluoroethylene (5 wt%) and acetylene black (15 wt%) and smearing the resulting mixture onto nickel foam using a scraper. Each nickel foam surface exhibited about 5–10 mg of electroactive material and had a square surface area of about 1 cm^2. The fabricated electrodes were dried at 60 °C for 10 h and then pressed under a pressure of 5 MPa.

The electrochemical properties of the fabricated electrodes were tested by cyclic voltammetry (CV) and galvanostatic charging/discharging (GCD). The specific capacitance Cs was calculated from the GCD curves by equation (1):

$$Cs = (I \times t)/(\Delta U \times m) \quad (1)$$

where I represents the discharge current, t corresponds to the discharge time, m represents the composite mass, and ΔU represents the voltage window.

3. RESULTS AND DISCUSSION

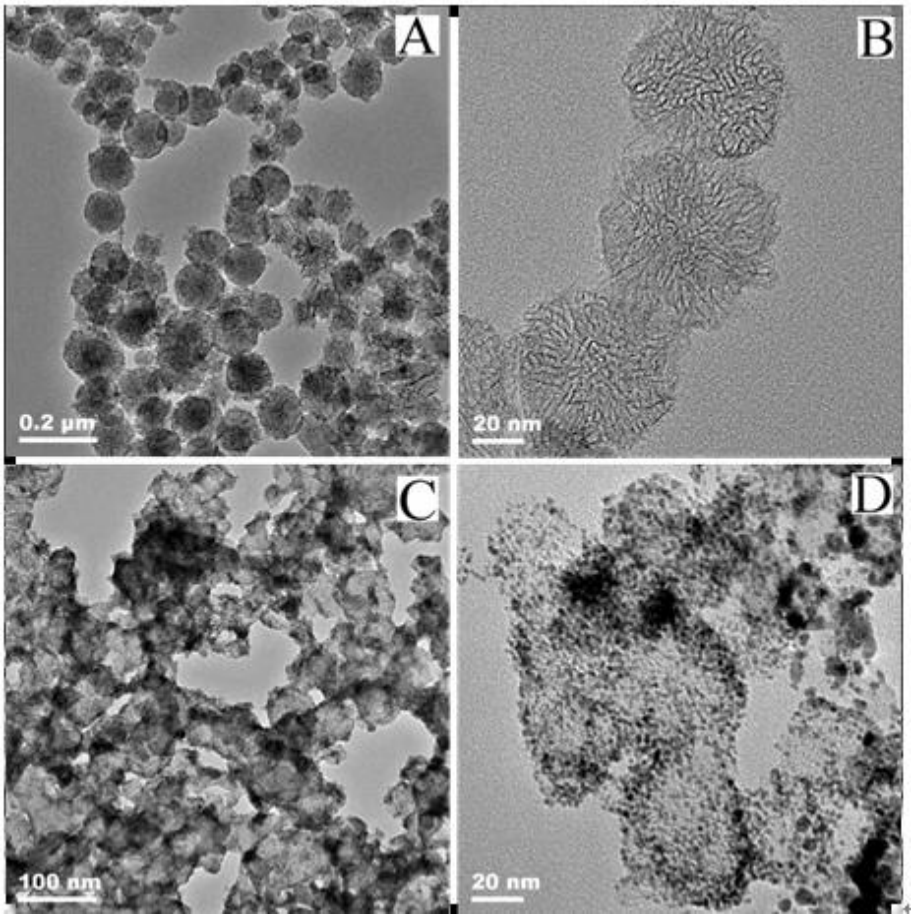

Figure 2. TEM images of SWCNHs and Pt/MnO_2@SWCNH at different magnifications.

Typical TEM images of SWCNHs and the Pt/MnO_2@SWCNH composite are shown in Figure 2. Figure 2A and 2B display TEM images of the SWCNHs at magnifications of 200 and 20 nm, respectively. The SWCNHs exhibited no obvious impurities on the surface, indicating that the purification by acidification was effective. SWCNHs adopted a uniformly distributed dahlia-like structure with a diameter of 60–80 nm and showed no aggregation. Figure 2C, 2D shows images of the Pt/MnO_2@SWCNH composite at magnifications of 100 and 20 nm, respectively. The Pt/MnO_2 nanoparticles were 2–5 nm in diameter and uniformly distributed on the surface of the SWCNHs. The SWCNHs maintained the dahlia-like cluster structure and showed no obvious change in the size after composite formation with Pt/MnO_2 nanoparticles, which proved that these small particles were not tightly packed on the SWCNH surface to form a shell. Instead, the Pt/MnO_2 nanoparticles were mainly distributed in the interstices of the horn structure to form a three-dimensional conductive network. The Pt/MnO_2@SWCNH microstructure is not only conducive to the rapid ion diffusion in the electrode but

also instrumental in increasing the contact area between MnO_2 and the conductive network formed by the Pt nanoparticles and the SWCNH substrate, providing more electron transfer pathways.[25]

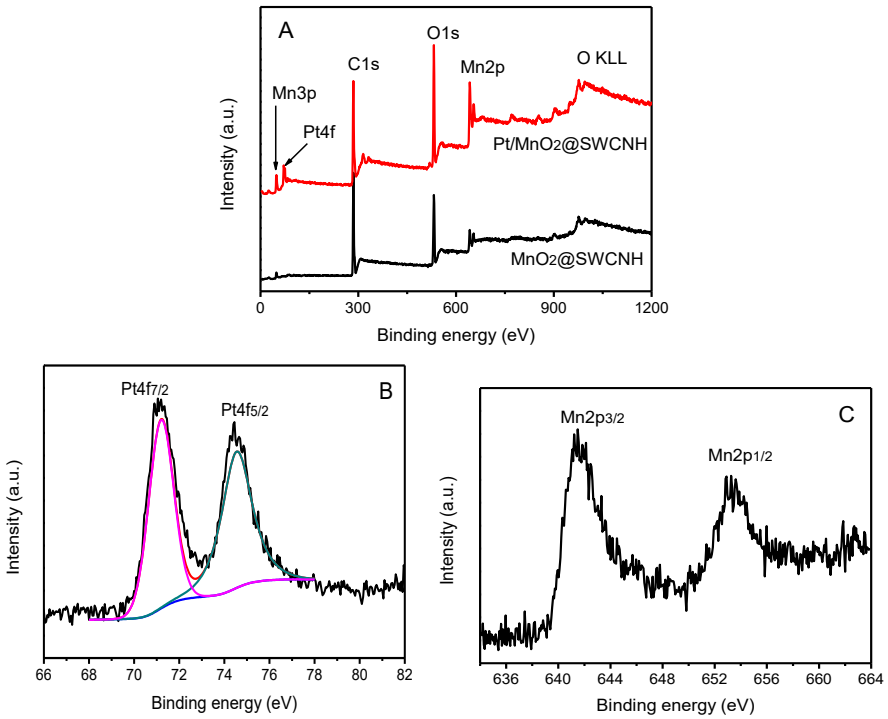

Figure 3. (A) XPS survey spectra of MnO_2@SWCNH and Pt/MnO_2@SWCNH. High-resolution XPS spectra of (B) Pt 4f and (C) Mn 2p.

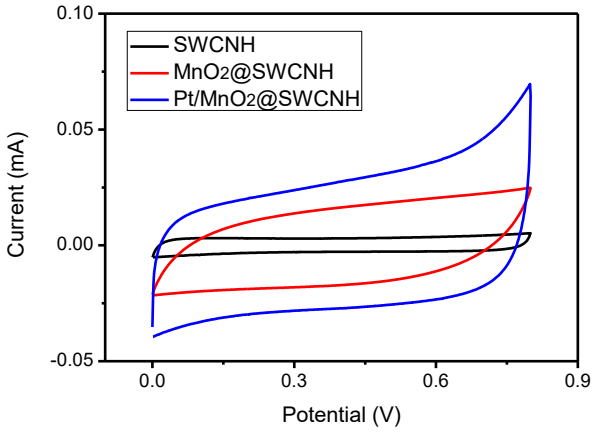

Figure 4. CV curves of electrodes modified with SWCNHs, MnO_2@SWCNH composite, or Pt/MnO_2@SWCNH composite at a scan rate of 10 mV/s.

Figure 3A shows the XPS spectra of MnO_2/SWCNH and Pt/MnO_2@SWCNH, exhibiting both the characteristic peaks of C1s, O1s, Mn2p, and Mn3p. In addition, the spectrum of Pt/MnO_2@SWCNH shows the Pt 4f peak at a binding energy of 73 eV. The high-resolution XPS spectrum of Pt 4f is shown in Figure 3B. The Pt 4f peak is split into two peaks, corresponding to Pt 4f7/2 and Pt 4f5/2 at binding energies of 71.36 and 74.68 eV, respectively, indicating that Pt nanoparticles were successfully incorporated into the MnO_2/SWCNH composite.[26] The high-

resolution XPS spectrum of Mn 2p (Figure 3C) shows the peaks of Mn 2p3/2 and Mn 2p1/2 at 641.91 and 653.20 eV, respectively, with an energy difference of 11.69 eV, which is consistent with the results reported in literature.[27] In conclusion, our results proved that the Pt/MnO_2@SWCNH composite was successfully prepared.

The electrochemical performance of the electrode materials was investigated by cyclic voltammetry at a scan rate of 10 mV/s, as shown in Figure 4. SWCNH exhibited a rectangular CV curve, indicating ideal double-layer behavior.[28] The CV curves of MnO_2@SWCNH and Pt/MnO_2@SWCNH were both quasi-rectangular with poorly defined broad peaks, indicating double-layer contribution of the SWCNHs and pseudo-capacitive contribution of MnO_2.[29] Since the specific capacitance of the electrode is directly proportional to the area under the CV curve [30], the specific capacitance of the Pt/MnO_2@SWCNH composite electrode is obviously larger than that of the MnO_2@SWCNH composite as well as that of pure SWCNHs.

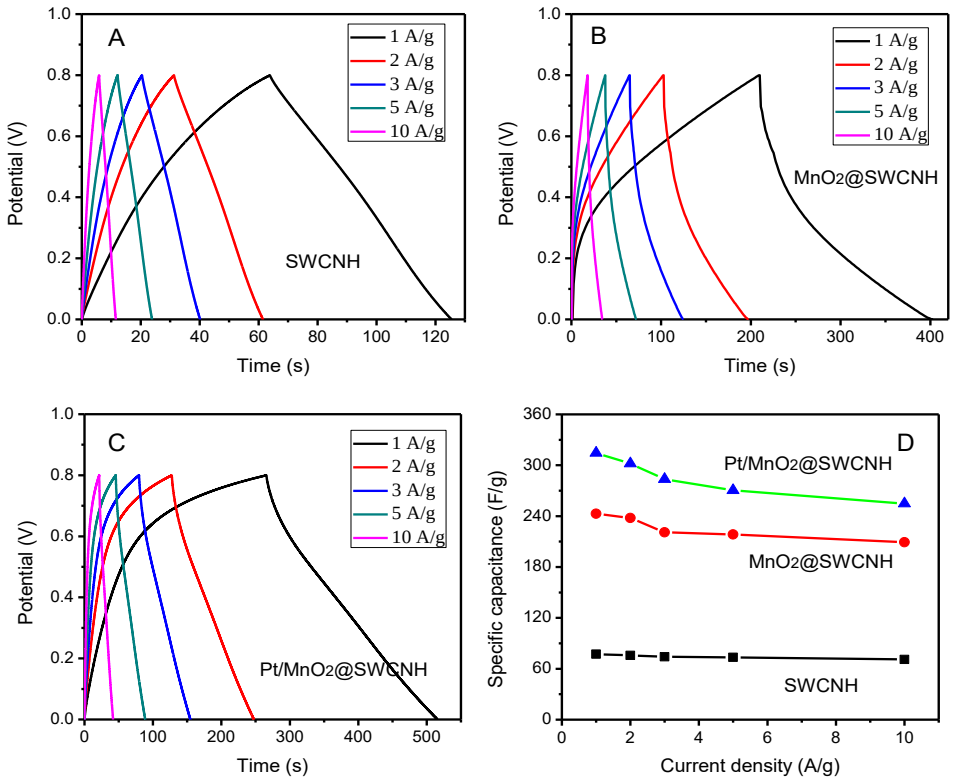

Figure 5. Galvanostatic charge/discharge curves of (A) SWCNH, (B) MnO_2@SWCNH, and (C) Pt/MnO_2@SWCNH composite electrodes at current densities of 1, 2, 3, 5, and 10 A/g. (D) Variation of the specific capacitance of SWCNH, MnO_2@SWCNH, and Pt/MnO_2@SWCNH composite electrodes with the current density.

Figure 5 shows the galvanostatic charge/discharge (GCD) curves and the specific capacitance of the electrode materials at different current densities. Figure 5A shows the constant-current charge/discharge curves of the SWCNH electrode at current densities of 1, 2, 3, 5, and 10 A/g. The curves at different current densities exhibited isosceles triangle shapes, and no IR drop was observed.

At current densities of 1, 2, 3, 5, and 10 A/g, the electrochemical capacitance of the SWCNH electrode was 77.3, 75.8, 74.2, 73.4, and 71.1 F/g, respectively. These results proved that the SWCNHs provide a three-dimensional spatial network structure for electron transport, ensuring a high conductivity and good rate performance.[31] Figure 5B shows the constant-current charge/discharge curves of the MnO_2@SWCNH composite electrode at current densities of 1, 2, 3, 5, and 10 A/g. The corresponding electrochemical capacitance of the MnO_2@SWCNH electrode was higher than that of the SWCNH electrode with values of 242.8, 237.9, 221, 218.5, and 209.2 F/g, respectively, due to the additional pseudo-capacitance of MnO_2. The IR drop of the MnO_2@SWCNH composite electrode was increased compared to that of the SWCNH electrode, which is due to the poor conductivity of MnO_2.[32] The GCD curves of Pt/MnO_2@SWCNH are shown in Figure 5C. At current densities of 1, 2, 3, 5, and 10 A/g, the corresponding electrochemical capacitance of Pt/MnO_2@SWCNH was 314.5, 301.9, 283.5, 270.5, and 254.8 F/g, respectively. The significant increase in capacitance compared with the SWCNH and MnO_2@SWCNH electrodes is attributed to the nanoscale contact between MnO_2 and Pt nanoparticles and the SWCNH substrate, which offers more electron transfer pathways. Moreover, the IR drop of the Pt/MnO_2@SWCNH electrode was significantly decreased compared with that of the MnO_2@SWCNH electrode, indicating that the Pt nanoparticles effectively decreased the electrode resistance. [33] Figure 5D shows the variation of the specific capacitance of the SWCNH, MnO_2@SWCNH, and Pt/MnO_2@SWCNH composite electrodes with the current density. As the current density increased to 10 A/g, the capacitance retention of the SWCNH, MnO_2@SWCNH, and Pt/MnO_2@SWCNH electrodes was 91.98%, 86.16%, and 81.02%, respectively. These results showed that the Pt/MnO_2@SWCNH composite electrode maintained a high capacitance at a high current density, indicating a good rate performance.

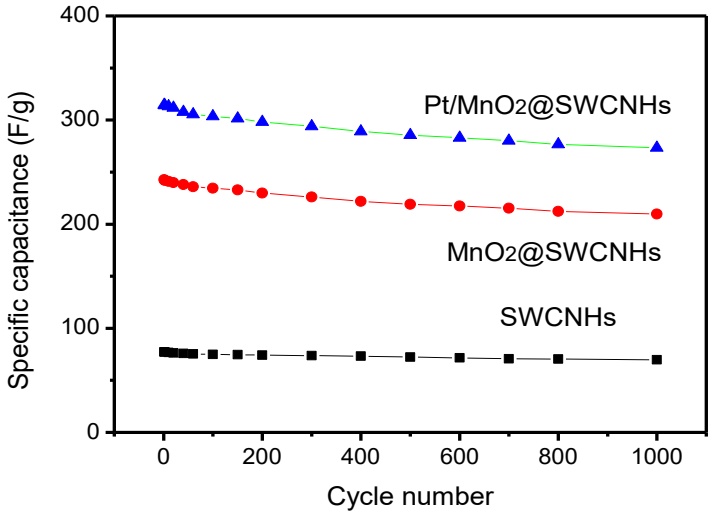

Figure 6. Cycle performance of SWCNH-, MnO_2@SWCNH-, and Pt/MnO_2@SWCNH-modified electrodes at a current density of 1 A/g.

The cycle stability is an important characteristic of the performance of supercapacitors. The cycle stabilities of the as-fabricated SWCNH, MnO_2@SWCNH, and Pt/MnO_2 @SWCNH electrodes at a current density of 1 A/g are demonstrated in Figure 6. After 1000 cycles, the specific capacitance

decreased from 77.3 to 69.68 F/g (90.14% capacitance retention) for the SWCNH electrode, from 242.8 to 209.6 F/g (86.33% capacitance retention) for the MnO_2@SWCNH composite electrode, and from 314.5 to 273.28 F/g (86.89% capacitance retention) for the Pt/MnO_2@SWCNH composite electrode. These results demonstrate an excellent cycle stability for all the samples, indicating that no serious structure change occurred after 1000 charge/discharge cycles. A possible reason is the formation of a stable three-dimensional network structure due to the strong adhesion of the MnO_2 and Pt nanoparticles to the SWCNH substrate. [34]

Table 1. Comparison of the capacitance of reported electrodes modified with Mn-based composites and the Pt/ MnO_2@SWCNH composite.

Electrode Materials	Electrolyte	Cs (F/g)
GO–MnO_2 nanocomposites [35]	1 M Na_2SO_4	216
CNFs/MnO_2 [36]	1 M Na_2SO_4	151.1
MnO_2@NCNTs@MnO_2 [37]	1 M Na_2SO_4	253.1
MnO_2 NSAs@VCFs [38]	1 M Na_2SO_4	115.3
Hollow MnO_2 nanofibers [39]	1 M Na_2SO_4	291.0
MnO_2/N-RGO[40]	1 M Na_2SO_4	275.2
rGO /MnO_2/CB[41]	0.5 M Na_2SO_4	209
Pt/MnO_2@SWCNH (this work)	1 M Na_2SO_4	314.5

GO: graphene oxide, CNFs: carbon nanofibers, NCNTs: nitrogen doped carbon nanotubes, NSAs: nanosheet arrays, VCFs: vapor grown carbon fibers, rGO: reduced graphene oxide CB: carbon black

To further demonstrate the advantages of the Pt/MnO_2@SWCNH composite, we compared its capacitance with that of reported electrodes modified with Mn-based composites. As shown in Table 1, our Pt/MnO_2@SWCNH composite exhibits an excellent performance with superior specific capacitance, which is ascribed to the unique cluster nanostructure of the SWCNHs and the three-dimensional conductive network formed by the SWCNHs and the Pt particles, resulting in more ion diffusion paths and electron transfer paths.

4. CONCLUSIONS

Herein, we report a high-performance supercapacitor electrode of SWCNHs decorated with MnO_2 and Pt nanoparticles prepared by a simple *in situ* synthesis method. The MnO_2 and Pt

nanoparticles were distributed in the interstices in the horn structure of the SWCNH substrate to form a three-dimensional conductive network. Electrochemical studies indicated that the as-prepared Pt/MnO_2@SWCNH composite has a high capacitance of 314.5 F/g and a long cycle life with 86.89% capacitance retention after 1000 charge/discharge cycles at a current density of 1 A/g. This outstanding electrochemical performance makes the Pt/MnO_2@SWCNH composite electrode a promising candidate for supercapacitor applications.

ACKNOWLEDGMENTS
The authors thank the Foundation of Jiangxi Educational Committee (GJJ170427, GJJ170437), the NSF of Jiangxi (20181BAB203012), the Foundation of East China University of Technology (DHBK2016110), and the Innovation Fund Designated for Graduate Students of East China University of Technology (DHYC-201914) for financial support.

References

1. Y. Qian, F. Gao, L. Du, Y. Zhang, D.Q. Tang and D.Z. Yang, *Biosens Bioelectron.*, 74 (2015) 483.
2. X.J. Liao, J.J. Luo, J. Wu, T.T. Fan, Y. Yao, F.L. Gao and Y. Qian, *Journal of Electroanalytical Chemistry*, 829 (2018) 129.
3. Y. Qian, D.Q. Tang, L.L. Du, Y.Z. Zhang, L.X. Zhang and F.L. Gao, *Biosens. Bioelectron.*, 64 (2015) 177.
4. F.L. Gao, Y. Qian, L. Zhang, S.Z. Dai, Y.F. Lan, Y. Zhang, L.L. Du and D.Q. Tang, *Biosenors. Bioelectron.*, 71 (2015) 158.
5. Y. Qian, T.T. Fan, P. Wang, X. Zhang, J.J. Luo, F.Y. Zhou,Y. Yao, X.J. Liao, Y.H. Li and F.L. Gao, *Sensors and Actuators B.*, 248 (2017) 187.
6. Y. Qian, T.T. Fan, Y. Yao, X. Shi, X.J. Liao, F.Y. Zhou and F.L. Gao, *Sensors and Actuators B.*, 254 (2018) 483.
7. T. Zhu, J.B. Ding, Q. Shao, Y. Qian and X.Q. Huang, *ChemCatChem.*, 11(2019) 689.
8. M.W. Zhu, Q. Shao, Y.C. Pi, J. Guo, B. Huang, Y. Qian and X.Q. Huang, *Small*, 13 (2017) 1701295.
9. M.W. Zhu, Q. Shao, Y. Qian and X.Q. Huang, *Nano Energy* 56 (2019) 330.
10. Y. Qian, C.L. Huang, R. Chen, S.Z. Dai and C.Y. Wang, *Int. J. Electrochem. Sci.*, 11 (2016) 7453.
11. R. Dubey and V. Guruviah, *Ionics*, 25 (2019) 1419.
12. A. Berrueta, A. Ursúa, I. S. Martín, A. Eftekhari and P. Sanchis, *IEEE Access*, 7 (2019) 50869.
13. V. V. N. Obreja, *Physica E*, 40 (2008) 2596.
14. D.W. Wang, Z.M. Lu, and L. Xu, *Journal of Materials Science*, 55 (2020) 7477.
15. A. Borenstein, O. Hanna, R. Attias, S. Luski, T. Brousse and D. Aurbach, *J. Mater. Chem. A*, 5 (2017) 12653.
16. P. Ju, Z. Zhu, X. Shao, S. Wang, C. Zhao, X. Qian and C. Zhao, *J. Mater. Chem. A*, 5 (2017) 18777.
17. Y. Qian, S.B. Lu, F.L. Gao, *Journal of Materials Science*, 46 (2011) 3517.
18. B. Huang, C.L. Huang, Y. Qian, *Int. J. Electrochem.Sci.*, 12 (2017) 11171.
19. N. Jabeen, Q. Xia, S. V. Savilov, S. M. Aldoshin, Y. Yu and H. Xia, *ACS Appl. Mater. & Inter.*, 8 (2016) 33732.
20. X. Du, *Int. J. Electrochem. Sci*., 14 (2019) 4195.
21. T. Jin, C. Liu, M. Zhou, S. Chai, F. Chen, Q. Fu, *Composites Part A*, 68 (2015) 193.
22. B. He, Y. Shi, Y. Liang, A. Yang, Z. Fan, L. Yuan, X. Zou, X. Chang, H. Zhang, X. Wang, W. Dai, Y. Wang and Q. Zhang, *Nat. Commun.*, 9 (2018) 2393.
23. A.S.D. Sandanayaka, O. Ito, T. Tanaka, H. Isobe, E. Nakamura, M. Yudasaka and S. Iijima, *New J. Chem.*, 33 (2009) 2261.
24. H.J. Jung, Y.J. Kim, J.H. Han, M. Yudasaka, S. Iijima, H. Kanoh, Y.A. Kim, K. Kaneko and C.M.

Yang, *J. Phys. Chem. C*, 117 (2013) 25877.
25. J. B. Shein, L. M. H. Lai, P. K. Eggers, J. J. Gooding, *Langmuir*, 25 (2009) 11121.
26. M. Wang, J. Chen, X. Liao, Z. Liu, J. Zhang, L. Gao, Y. Li, *Int. J. Hydrogen Energy*, 39 (2014) 14581.
27. S. Ramesh, K. Karuppasamy, S. Msolli, H.S. Kim, H.S. Kim and J.H. Kim, *New J. Chem.*, 41 (2017) 15517.
28. J. Yin, L. Qi, H. Wang, *Electrochim. Acta*, 88 (2013) 208.
29. P.-C. Gao, P. A. Russo, D. E. Conte, S. Baek, F. Moser, N. Pinna, T. Brousse, F. Favier, *ChemElectroChem*, 1 (2014) 747.
30. N. Nagarajan, H. Humadi, I. Zhitomirsky, *Electrochim. Acta*, 51 (2006) 3039.
31. S. Ren, Y. Yang, M. Xu, H. Cai, C. Hao, X. Wang, *Colloids Surf. A*, 444 (2014) 26.
32. M. S. Javed, J. Chen, L. Chen, Y. Xi, C. Zhang, B. Wan, C. Hu, *J. Mater. Chem. A.*, 4 (2015) 667.
33. W. Oelßner, F. Berthold, U. Guth, *Mater. Corros.*, 57 (2006) 455.
34. X. Zhang, W. Wang, A. Wang, Y. Huang, K. Yuan, Z. Yu, J. Qiu, Y. Yang, *J. Mater. Chem. A*, 2 (2014) 11660.
35. S. Chen, J. Zhu, X. Wu, Q. Han and X. Wang, *ACS Nano*, 4 (2010) 2822.
36. P. Ning, X. Duan, X. Ju, X. Lin, X. Tong, X. Pan, T. Wang and Q. Li, *Electrochim. Acta*, 210 (2016) 754.
37. L. Chen, M. Zhang, X. Yang, W. Li, J. Zheng, W. Gan and J. Xu, *J. Alloys Compd.*, 695 (2017) 3339.
38. S.C. Sekhar, G. Nagaraju, S.M. Cha and J.S. Yu, *Dalton Trans.*, 45 (2016) 19322.
39. K. Xu, S. Li, J. Yang and J. Hu, *J. Colloid Interface Sci.*, 513 (2018) 448.
40. J. Mei and L. Zhang, *Electrochimica Acta*, 173 (2015) 338.
41. J. Chen, Y. Wang, J. Cao, Y. Liu, J.-H. Ouyang, D. Jia and Y. Zhou, *Electrochimica Acta* 182 (2015) 861.